Sizing and Optimization of Novel General Aviation Vehicles and Propulsion System Architectures

Gokcin Cinar*, Yu Cai†, Imon Chakraborty‡, Dimitri N. Mavris§
Aerospace Systems Design Laboratory, School of Aerospace Engineering,
Georgia Institute of Technology, Atlanta, Georgia, 30332

The drive for more efficient flying vehicles in all categories may necessitate a significant departure from the tube-and-wing or rotary-wing norms that have been the mainstay of aviation for many decades. This poses challenges for predicting the aerodynamic characteristics and the weight build-up of such unconventional vehicles in early design phases. Additionally, the design and assessment of advanced/unconventional all-electric or hybrid-electric propulsion system architectures require consideration of degrees-of-freedom and trade-offs that do not arise for conventional purely fuel-powered architectures. Thus, there is a need for a flexible vehicle sizing, trade-off, and optimization capability that is not limited to a single vehicle configuration (e.g., fixed-wing, rotary-wing) or propulsion system architecture. To be suitable for the early design phases, such a framework must evaluate relatively quickly, not require extensive definition of the vehicle, and lend itself to customizable design optimization setups. This paper describes the initial creation of such a capability and demonstrates its application to design trade-offs for a General Aviation vehicle with an advanced propulsion system architecture.

I. Introduction

A review of flight vehicle designs over the past few decades shows that the vast majority of them fall into a fairly small number of geometric configurations and propulsion system designs. A by-product of this is the availability of a large volume of historical data that has allowed the development of regression relationships for making early predictions of, for instance, the weights of major vehicle components [1, 2]. However, the applicability of such relationships may be limited for vehicle configurations that differ significantly from the norm, which would necessitate alternative weight build-up approaches.

Additional challenges arise when all-electric or hybrid-electric propulsion system architectures are considered. The well-documented large difference in the energy densities of conventional fuels (≈42.80 MJ/kg [3]) and state-of-the-art battery systems (≈0.76 MJ/kg [4]) makes electric aircraft significantly more weight-sensitive than their conventional counterparts. However, current technological feasibility aside, it is also more challenging to size and analyze such propulsion systems. For instance, with hybrid-electric architectures, propulsion system fuel/energy requirements and system mass penalties depend on power and energy sizing and management strategies, which introduce additional degrees-of-freedom into the design problem.

Such challenges notwithstanding, notable advances in vehicle configuration and electrified propulsion system architectures are occurring in the General Aviation (GA) category. The 2-seat Pipistrel Alpha Electro trainer is powered by a 65 kW electric motor (≈ 5 kW/kg including inverter and gearbox), and a lithium battery pack which allows up to 1 hour endurance with an extra 30 minutes reserve and a 200 km cruise range [5–7]. The twin-engined, 2-seat Airbus E-Fan 2.0 demonstrator [8], which uses a 29 kWh lithium-ion battery pack (207 Wh/kg per cell) to power two 30 kW motors with a 270V system, also has a 1-hour endurance, but only one-third the operating cost of a piston-engine light aircraft. The 1,000 kg electric Extra 330LE aerobatic aircraft demonstrator is powered by Siemens 260 kW direct-drive electric

*Senior Graduate Researcher, ASDL, School of Aerospace Engineering, Georgia Tech, AIAA Student Member
†Graduate Researcher, ASDL, School of Aerospace Engineering, Georgia Tech, AIAA Student Member
‡Research Engineer II, ASDL, School of Aerospace Engineering, Georgia Tech, AIAA Member
§S.P. Langley Distinguished Regents Professor and ASDL Director, School of Aerospace Engg., Georgia Tech, AIAA Fellow

motor weighing 50 kg, can fly 30 minutes per charge, and achieved the world record of the fastest-climbing electric aircraft that weight between 500-1,000 kg by climbing to 3,000 m in 4 minutes and 22 seconds [9, 10].

Several other urban air mobility concepts exist that consist of multiple propellers or rotors driven by electric motors enabling vertical take-off and landing (VTOL). Aurora's on-demand eVTOL (Electric Vertical Takeoff and Landing) concept includes eight lift rotors for VTOL along with one cruise propeller for high-speed forward flight and is designed for short-haul urban transport of passengers or cargo [11]. The XV-24A, another Aurora VTOL concept, employs a hybrid electric distributed propulsion system powered by lithium batteries and is aimed at high-speed forward flight with a sustained flight speed of 300-400 knots and 15% higher hover efficiency compared to conventional helicopters [12, 13]. Uber has developed three eVTOL Common Reference Models (eCRMs) for its Uber Elevate project, which is visioned to be a 4-5 passenger VTOL aircraft sized to fly 60 nautical miles (25 nautical miles nominal flight distance) running on battery energy with 300Wh/kg of specific energy at the pack level [14]. The 2-seat Volocopter 2X, which uses 18 rotors powered by 9 independent high capacity lithium-ion batteries, has a maximum range of 27 km at a cruise speed of 70 km/h and a maximum flight time of 27 minutes at a cruise speed of 50 km/h [15]. The 5-passenger Lilium Jet, another electric VTOL aircraft, comprises a rigid winged body with 12 flaps, each one carrying three tilting electric jet engines. It does not require gearboxes, foldable or variable pitch propellers, water-cooling, or aerodynamic steering flaps, and its first manned flight is scheduled for 2019 [16]. These recent demonstrations indicate that GA may indeed be the first avenue for large-scale introduction and maturation of such novel aircraft configurations with electric and hybrid-electric propulsion system designs.

There have been some conceptual studies and research into developing sizing approaches for such vehicles. For instance, Nam et al. [17, 18] proposed a generalized aircraft sizing formulation applicable to non-traditional energy sources and propulsion systems. This formulation follows a power-based approach based on multiple "power-paths" that make up the propulsion system when integrated and where each subsystem is represented by its individual specific energy, specific power, and efficiency. Pornet et al. [19] presented a methodology for sizing and performance assessment of hybrid-electric aircraft by extending traditional thrust and fuel-flow look-up tables to include electrical system characteristics; specifically by including the required electric power as an additional output parameter. However, this methodology is only for sizing the power systems in parallel hybrid electric architectures and not for determining an optimum hybridization factor. Isikveren et al. [20] argued that if the electric propulsion architecture is sized for low-speed operations (specifically, take-off and initial climb), there will be a dramatic weight penalty due to the oversized battery. Hence, energy management optimization should be performed during vehicle sizing. Perullo and Mavris [21] proposed a hybrid-electric design environment by combining conceptual design tools with energy management optimization for a full mission. They decouple the sizing process from the mission analysis so that the optimization takes place for two problems: (i) high level design parameters (e.g. aspect ratio, engine cycle parameters, etc.) and (ii) degrees of freedom available to the system during a mission (e.g. power split from multiple sources, etc.) using model predictive control technique. Moore and Fredericks [22] stated that compared to a traditional propulsion architecture with a few large diameter propellers on the same aircraft design, distributed electric propulsion architecture (i.e., distributing many small diameter propellers over the wing) results in the highest propeller induced velocities and the greatest lift augmentation, which in turn provides high aerodynamic efficiency and the ability to cruise at higher speeds with almost an optimum maximum lift coefficient. Borer et al. [23] supported this finding by demonstrating these advantages for the case of a retrofitted light twin-engine training aircraft with two types of distributed electric propulsion architecture. Borer et al. performed an initial sizing process to demonstrate up to 5 times cruise efficiency over the baseline aircraft, but without any hard mission requirements.

There are several aircraft sizing and analysis tools in literature that can be used for mission performance analysis for conventional fuel burning aircraft, such as the Flight Optimization System (FLOPS) tool developed by NASA [24]. However, this is not the case for electric and hybrid electric aircraft (EA/HEA) concepts. While FLOPS is capable of performing limited EA/HEA analysis, it only allows for a single propulsion type to be in use at any given point of time during the mission analysis. This means that the aircraft can only operate in full-electric or conventional mode (but not hybrid-electric), although the operation schedules are interchangeable [24, 25]. While some cumbersome workarounds (involving performing additional calculations outside FLOPS) have been reported in literature, the FLOPS tool in current form is not ideally suited for the analysis of hybrid-electric propulsion systems.

To summarize, the main challenges associated with the EA and HEA and their design process are: (i) lack of historical data and readily available physics-based models for the Electrical Power Generation

and Distribution System (EPGDS), (ii) interdependency among aircraft sizing, performance, subsystem sizing, and architectural decisions, (iii) the need to modify the traditional sizing methods to account for new propulsion systems and geometric configurations, and (iv) concurrent performance optimization for both on-design and off-design missions.

The goal of this paper is to present and demonstrate a sizing, analysis, and optimization framework that addresses the above-mentioned challenges, for the specific case of a novel GA vehicle and propulsion system. This paper will demonstrate the developed methodology with respect to a specific baseline GA aircraft similar to the Cessna 172.

The remainder of the paper is organized as follows: Section II describes the hybrid electric propulsion system architectures of interest. Section III introduces the generalized mission performance analysis. Section IV describes the weight estimation approach, while Section V lays out the sizing and synthesis steps. Section VI introduces the aircraft and mission optimization approach. Section VII provides the results and discussions for an example application of the developed framework. Section VIII concludes the paper and identifies some avenues for future work.

II. Baseline Aircraft and Architecture Selection

The baseline aircraft with conventional propulsion system was chosen (mainly based on ready data availability) to be a low-speed four-seater GA aircraft powered by a single piston engine, similar to the Cessna 172 [26]. Data pertaining to the baseline aircraft was first used to validate the developed sizing and weight estimation framework. The vehicle sizing was performed to meet the point performance characteristics of the baseline aircraft, and the design mission was defined to reproduce the payload-range diagram of the baseline. Subsequently, the propulsion system architecture was modified to accommodate an electric propulsion branch. To develop the necessary relationships for the propulsion system architectures of interest within the presented framework, a brief overview of prominent hybrid electric architectures is provided in the following sections.

A. Major Classification of Hybrid Electric Architectures

Hybrid-electric propulsion architectures incorporate an electric power source and a fuel burning engine (e.g., gas turbine or internal combustion engine). Two prominent hybrid electric architecture categories exist in literature, differing in the way power generation and distribution subsystems are connected to each other: (i) series configuration (Figure 1(a)) and (ii) parallel configuration (Figure 1(b)). It should be noted that other hybrid electric propulsion configurations can be created by incorporating these two types simultaneously, such as series-parallel and complex configurations [27, 28].

In the series hybrid electric configuration, the mechanical energy at the output of the fuel burning engine is first converted into electricity by the generator. This electrical energy can be used to charge the battery or to power the electric motor(s). One of the advantages of the series architecture is that the fuel burning engine is decoupled from the transmission system and thus it can run at its peak efficiency independent of the speed of the transmission system. It also has the advantage of flexibility in terms of locating the engine-generator set. The powertrain is also not as complex as some other architectures.

As evident from Figure 1(a), there are three propulsion devices (fuel burning engine, generator, and electric motor) in this architecture. Each needs to be sized for the maximum sustained power for high performance flight, which results in an increased weight penalty. Although a gearbox can be integrated to amplify torque and improve the performance of the motor and hence reduce its size, the motor must still be significantly more powerful than a motor used in an equivalent parallel hybrid architecture [27, 28]. Further, the weight penalty of the gearbox must be considered.

In the parallel hybrid electric configuration, the fuel burning engine and the electric motor are coupled to the shaft via two clutches, as seen in Figure 1(b). With this arrangement, the electric motor and the fuel burning engine can supply the propulsion power either simultaneously or separately. The main advantage of this configuration over the series configuration is that it may be possible to downsize either the engine or the motor (or both) while still achieving the same maximum shaft-power. Further, there is no need for a generator in parallel architecture. The main disadvantage is that this architecture increases the control complexity, requires more complex and expensive transmission system, as well as mechanical couplings [27, 28].

B. Overview of Propulsion System Architecture Analyzed

Within the scope of this paper, a parallel hybrid electric configuration was selected to demonstrate the proposed sizing approach. This allows power optimization strategies as well as "electric propulsion only" and "fuel burning engine only" scenarios to be tested and analyzed.

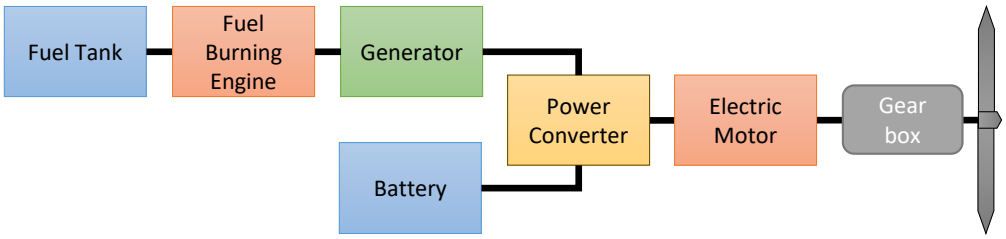

(a) Series hybrid electric propulsion

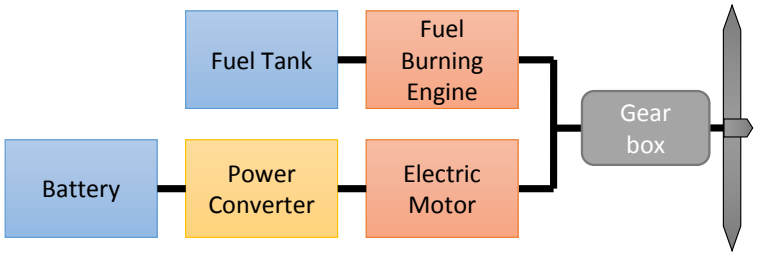

(b) Parallel hybrid electric propulsion

Figure 1. Notional components and power-flow for (a) series hybrid electric propulsion, (b) parallel hybrid electric propulsion [27]

III. Mission Performance Analysis

The basis of the mission performance analysis approach derives from energy methods, more specifically what is referred to as the *energy reservoir analogy* [29, 30]: the fact that the rates at which the propulsion system and aerodynamic drag respectively supply and remove energy from the vehicle system yields the rate of change of its total mechanical energy (sum of kinetic and gravitational potential energies):

$$\vec{T} \cdot \vec{V} + \vec{D} \cdot \vec{V} = \frac{d}{dt}\left(Wh + \frac{1}{2}\frac{W}{g}V^2\right) \tag{1}$$

In Eq. 1, the dot product of thrust T and velocity V is referred to as the propulsive power. For the case where the thrust vector is exactly or closely aligned with the velocity vector, the simplification $\vec{T} \cdot \vec{V} = TV$ occurs. Henceforth, these two terms are shown as grouped (TV). Since the drag force, by definition, is aligned opposite to the velocity vector, the simplification $\vec{D} \cdot \vec{V} = -DV$ occurs. The rate of energy dissipation to drag is henceforth expressed as the product of drag and velocity, (DV).

The difference between (TV) and (DV) is called the *excess power*, and can be modulated through the vehicle's control effectors to change the energy state of the aircraft, through a change of kinetic and/or gravitational potential energy. Depending on the flight phase and the intended manner in which it is to be flown, the excess power can be suitably apportioned to kinetic and potential energy rates, thus allowing computation of vehicle acceleration (dV/dt) and rate of climb (dh/dt). The numerical integration of these time derivatives along with time derivatives of vehicle mass and energy consumption rate (described subsequently) form the core of the mission performance analysis method.

A. Characterization of Aerodynamic Drag

The rate of energy dissipation due to aerodynamic drag (DV) is modeled using the drag characteristics of the vehicle in question. The general approach (also followed in this work) is to model the aerodynamic efficiency

of the vehicle through a *drag polar* which expresses the non-dimensional drag coefficient C_D as a function of the non-dimensional lift coefficient C_L, i.e., $C_D = f(C_L, \ldots)$. The (DV) product is then given by

$$(DV) = \frac{1}{2}\rho V^3 S_{ref}\ C_D, \tag{2}$$

where ρ is air density and S_{ref} the reference area based on which the drag coefficient C_D is defined.

B. Characterization of Propulsion System Performance

The modeling of the propulsion system performance is embedded within a function Φ_{ps}, which is responsible for computing the propulsive power (TV), the rate of change of vehicle mass (dm/dt), and the rate of change of vehicle propulsion energy content (dE/dt).

$$\left[(TV), \frac{dm}{dt}, \frac{dE}{dt}\right] = \Phi_{ps}\left[(TV)_{dem}, h, M, \lambda, P_{np}, \ldots\right] \tag{3}$$

It should be noted that (i) if the propulsion system architecture or operation mode is such that no mass change occurs, then $dm/dt = 0$, and (ii) if the vehicle contains multiple energy sources, then the propulsion energy E comprises multiple elements: $E = \{E_1, \ldots, E_n\}$. To compute these output quantities, evaluation of the function Φ_{ps} requires the demanded propulsive power $(TV)_{dem}$, the flight condition (altitude h, Mach number M), the non-propulsive (secondary) power off-take P_{np}, and possibly other factors (represented by $\ldots$). With regard to the input quantities, the following should be noted:

1. The amount of power drawn from of each power source is dictated by the power split strategy employed during the phase of flight. The power split during a flight phase can be expressed by a *hybridization factor* vector, λ, which describes the ratio of the power supplied by each power source. In this work, two different definitions for the hybridization factor are employed depending on the mission segment, as further explained in Section III-D.

2. If the available power at a given flight condition exceeds the demanded power and no other operational constraints have not been reached, then the propulsive power is nominally equal to the demanded propulsive power, i.e., $(TV) = (TV)_{dem}$.

3. The manner in which the flight condition $(h,\ M)$ affects the propulsion system performance is highly dependent on the nature of the propulsion system architecture, i.e., the nature of power lapse (if present) and the impact of flight condition on propulsion system performance (which may affect both dm/dt and dE/dt).

4. Non-propulsive (secondary) power off-takes, the extraction of power from the propulsion system to satisfy vehicle power requirements other than that required for propulsion, always degrade propulsion system performance (affecting dE/dt and dm/dt for a given (TV)). If maximum available power is already demanded, then secondary power off-takes result in a reduction of the effective propulsive power output, and thus degradation in the point performance (dh/dt and/or dV/dt).

It should be noted that the above formulation can be used to model any propulsion system, including fuel-burning internal combustion and gas turbine engines, electrically powered systems, as well as hybrid systems (through varying relationships contained within Φ_{ps}).

C. Characterization of Propulsion Architecture

For hybrid propulsion systems, the propulsion performance varies for different architectures. To develop the necessary relationships within Φ_{ps} for the propulsion system architectures of interest, a set of definitions to reveal the relationship between the main electric power generation and distribution subsystems must be established. In this work, the propulsion system architecture operates through interactions among components falling into three main categories:

1. **Power source (PS):** includes any subsystem that generates primary (propulsive) power, such as an electric motor, internal combustion engine, turboprop engine, etc.

2. **Thrust source (TS):** includes any subsystem that generates thrust, such as a propeller.

3. **Energy source (ES):** includes any subsystem that stores energy to be used by the primary power sources, such as batteries, fossil fuel, fuel cells, etc.

For convenience and traceability, each distinctive source is given an identification number. For instance, for either configuration shown in Figure 1, the fuel inside the fuel tank can be labeled as ES 1 , battery as ES 2, fuel burning engine as PS 1, electric motor as PS 2, and propeller as TS 1. Once the components are distributed under these three categories, applicable inter-relationships are defined. This is performed by a set of matrices which contain information regarding component dependencies. These matrices are:

1. **Energy Source - Power Source Matrix:** This lays out which power source draws its energy from which energy source by logical comparisons.

2. **Thrust Source - Power Source Matrix:** This includes information on which power source is connected to which thrust source.

Each element a_{ij} of matrix A represents the relationship between a source identified by *Source* i and another source identified by *Source* j. For instance, for either configuration shown in Figure 1, the ES-PS matrix (A_{ESPS}) is a two-by-two identity matrix where rows represent the energy sources and columns represent the power sources. In matrix A_{ESPS}, $a_{1,1} = 1$ relates ES 1 (fuel) to PS 1 (fuel burning engine) through the logical value of 1 (true), whereas $a_{1,2} = 0$ depicts that no such relation exists for ES 1 (fuel) and PS 2 (electric motor) through the logical value of 0 (false).

Similarly, for either configuration shown in Figure 1, the TS-PS matrix (A_{TSPS}) is a 1×2 matrix where the row represents the thrust source and columns represent the power sources. It can easily be inferred from matrix A_{TSPS} that PS 1 (fuel burning engine) and PS 2 (electric motor) are connected to TS 1 (propeller) through $a_{1,1} = 1$ and $a_{1,2} = 1$, respectively.

$$A_{ESPS} = \begin{bmatrix} 1 & 0 \\ 0 & 1 \end{bmatrix}, \qquad A_{TSPS} = \begin{bmatrix} 1 & 1 \end{bmatrix}$$

Although the Thrust Source - Power Source Matrix shows which sources are connected together logically, it does not reveal any information about how they are connected physically, i.e, the propulsion system configuration. Hence, if any thrust source is run by more than one power source, at least one of the following matrices must be defined in addition to the Thrust Source - Power Source Matrix:

- Series Source Matrix: comprises the power sources connected in series
- Parallel Source Matrix: comprises the power sources connected in parallel

The three source categories and the related matrices are used within the propulsion system performance function to distribute the required power, thrust, and energy from each existing source. Defining the relations between different sources with the logical A_{ESPS} and A_{TSPS} matrices is convenient as the power, thrust, or energy from each source can be easily computed by multiplying the power, thrust, or energy in the powertrain by the matrix itself.

D. Mission Segment Functions

The mission segment functions calculate the vehicle performance for climb, cruise, and descent segments. For each of these segments, a segment profile can be generated by a user-defined altitude-velocity schedule, or by choosing an objective function to auto-create the most suitable profile. Each segment is discretized by a number of control points, henceforth referred as segment points. The vehicle state and performance are calculated at each one of these points. This information is carried on to the final output as the mission history, which lists the vehicle dynamics and performance as a function of time. The following sections describe the calculation methods used in each mission segment.

1. *Climb Segment*

Central to the climb segment performance computations are the concepts of energy height H_e and specific excess power P_s, which are defined as

$$H_e = h + \frac{V^2}{2g}, \qquad P_s = \frac{TV - DV}{W}. \tag{4}$$

which are related to the specific excess power P_s as

$$P_s = \frac{TV - DV}{W} = \frac{1}{W}\frac{d}{dt}\left(Wh + \frac{1}{2}\frac{W}{g}V^2\right) = \frac{dH_e}{dt}. \tag{5}$$

This allows the time interval Δt to achieve an energy height increment ΔH_e to be computed based on the average specific excess power $P_{s,avg}$ over that interval as

$$\Delta t = \frac{\Delta H_e}{P_{s,avg}} \tag{6}$$

Thus, the climb segment may be discretized in terms of energy height as well as in terms of altitude. Three types of climb profiles can be computed:

1. Velocity-scheduled climb profile: In this case, the segment is discretized in terms of altitude, with the target velocity (and, if desired, power setting) known as a function of altitude. This allows the specific power P_s to be computed at the start and end of each altitude interval. The corresponding time intervals are computed based on the average P_s over the altitude interval.

2. Time-optimal climb profile: The minimum time path, as seen from Eq. 6, is one that maximizes the specific excess power over the profile. At each energy height, the h-V (altitude-velocity) combination that achieves this is identified in order to construct the time-optimal path. The time required to transition between energy heights is then computed using Eq. 6.

3. Energy-optimal climb profile: By substituting Eq. 6 into the relationship $\Delta E = (dE/dt)\Delta t$, it can be shown that the minimum energy climb profile requires the maximization of the quantity $-P_s/(dE/dt)$ over the climb segment. The h-V combination that achieves this at each energy height is identified, and then Eq. 6 is used to compute the time required to transition between energy heights.

With the time intervals Δt between successive energy heights identified, the energy depletion and (if applicable) mass reduction can be computed as:

$$\Delta E = \left(\frac{dE}{dt}\right)_{avg} \Delta t, \qquad \Delta m = \left(\frac{dm}{dt}\right)_{avg} \Delta t. \tag{7}$$

It should be noted that the mass change Δm can have a potentially significant effect on climb performance (through impact on mean specific excess power $P_{s,avg}$). However, Δm cannot be computed until the time interval Δt (which depends on $P_{s,avg}$) has been computed. Therefore, the climb profile has to be evaluated iteratively until the relevant quantities converge to within a specified tolerance between successive iterations.

In the climb segment, the hybridization factor λ_i for a power source i is defined as the ratio of the desired output power (P_i) to its respective sea level rated power ($P_{SL,\,rated}$), as described in Eqn. 8. In that sense, each λ_i is independent from the utilization of the remaining power sources.

$$\lambda_{i,\,climb} = \frac{P_i}{P_{SL,\,rated}} \tag{8}$$

Note that the actual available power for a setting of $\lambda_{i,climb}$ depends on the lapse characteristics of the power source in question. Thus, for an IC engine, there will be a power lapse with altitude. However, this will not be the case for an electric motor.

2. *Cruise*

The cruise segment calculations start with identification of available information about velocity and altitude and continue with the definition of an objective function to optimize the cruise profile. There are three options: If neither the end altitude nor end speed are specified, then the velocity and altitude at each point in the segment are chosen to be those which would optimize the objective function. If only the end altitude or the end velocity is known, then the other can be selected such that the resulting altitude-velocity combination optimizes the objective function.

The cruise segment is discretized in terms of cruise distance. At each point in the segment, the velocity and/or altitude is updated to optimize the chosen objective function. There are two main profiles (hence two objective functions) to choose from: (i) best specific air range, (ii) best endurance.

1. Best specific air range cruise: Specific air range (SAR) is defined for traditional fuel consuming aircraft as the ratio of the distance flown per unit of fuel consumed (i.e., ds/dW_f). [31] However, this definition does not apply to aircraft which do not burn fuel and hence needs to be modified to include any type of propulsion system and energy source, regardless of fuel consumption. Since energy is the common measure of performance for both fuel burning and electric propulsion systems, the SAR definition can be modified as *the ratio of the distance flown per unit* ***energy*** *consumption.* This yields Eqn. 9:

$$\mathbf{SAR} = \frac{ds}{dE} = \frac{V}{dE/dt} \tag{9}$$

   The energy term E in Eqn. 9 represents the total amount of energy of all available energy sources. To maximize the aircraft range in the most efficient way possible, the optimum flight conditions (in terms of altitude and velocity) can be found by maximizing the right-hand-side of Eqn. 9.

2. Best endurance profile: For aircraft with conventional propulsion systems, endurance is defined as the amount of time that an airplane can stay in the air on one load of fuel [32]. Similar to the previous discussion about SAR, this definition can be generalized as *the amount of time that an airplane can stay in the air as limited by the total amount of* ***energy*** *on-board to spend.* This yields the following relationship:

$$\mathbf{dt} = \frac{dE}{dE/dt} \tag{10}$$

   In Eq. 10, the total amount of available energy at any given time is fixed. Hence, the best endurance profile can be obtained by minimizing the time rate of change of energy, dE/dt.

Similar to the climb segment, the cruise profile is obtained iteratively due to the effect of the change in aircraft mass Δm on the time rate of change of energy (dE/dt). The cruise segment definition of the hybridization factor differs from the one defined in the climb segment. In this segment, λ_i for each power source i is defined as a percentage of the required power (TV_{req}), as shown in Eq. 11. Therefore, the sum of λ_i must be equal to 1 for unaccelerated level flight at a given altitude and velocity.

$$\lambda_{i,\,cruise} = \frac{P_i}{TV_{req}} \tag{11}$$

3. *Descent*

The descent segment is first discretized within the specified initial and final altitudes according to the number of segment points. Then, a descent profile is chosen to calculate or optimize the vehicle state at each one of these points according to a chosen profile. There are four profile options for this segment: a given rate of descent, a given velocity, minimum equilibrium glide angle, or minimum rate of descent. Except for the first option, the rate of descent throughout the descent segment is not specified, and therefore the profile is obtained iteratively through energy height and specific excess power computations, just as discussed for the *climb segment.*

1. Specified rate of descent: The rate of descent (also known as the sink rate and shown as dh/dt with a negative value) can be specified as a varying or a constant value throughout the segment. In this case, the aerodynamic and propulsion system performance are simply calculated one segment point at a time, each time using the state of flight from the previous point.

2. Specified descent velocity: In this case, the segment is flown with the target velocity.

3. Minimum equilibrium glide angle: For an unpowered aircraft in descending flight , the equilibrium glide angle (θ) is strictly a function of lift-to-drag ratio, as shown in Eqn. 12. [32].

$$\tan\theta = \frac{1}{L/D} \tag{12}$$

It can easily be seen from Eq. 12 that the minimum equilibrium glide angle is obtained at maximum lift-to-drag ratio, $(L/D)_{max}$. As discussed previously, the lift-to-drag ratio for a given state of flight can be obtained from the drag polar of the vehicle.

To fly at $(L/D)_{max}$, the vehicle must fly at a specified velocity called the equilibrium glide velocity (V_∞) [32]. Although the equilibrium glide angle does not depend on altitude or wing loading, the equilibrium glide velocity does, as it can be seen from Eqn. 13. Therefore, at every point of the mission segment, V_∞ must be updated such that $(L/D)_{max}$ is achieved.

$$\mathbf{V}_\infty = \sqrt{\frac{2\cos\theta}{\rho_\infty}\frac{W}{S}} \tag{13}$$

4. Minimum rate of descent: The rate of descent is proportional to the power required for steady, level flight (DV), as given in Eq. 14. Therefore, the minimum rate of descent occurs at minimum (DV), which is obtained when $L^{3/2}/D$ is maximum. Similar to the previous case, the target lift-to-drag ratio does not depend on aircraft weight or altitude, and hence remains constant. However, the corresponding true airspeed does vary with weight. Therefore, the aircraft velocity is updated to give the target lift-to-drag ratio at each point in the segment. The remaining calculations (and iterations) are the same as the previous case. The resulting dh/dt is the minimum rate of descent.

$$\frac{\mathbf{dh}}{\mathbf{dt}} = \frac{DV}{W} \tag{14}$$

The hybridization factor λ definition for the descent segment can be the same as the cruise segment λ definition. This means that for an unpowered descent, *lambda* would be zero.

IV. Vehicle Weight Estimation

Vehicle weight estimation for sizing in the early design phases has typically been done with the help of regression relationships that were developed from historical data pertaining to existing aircraft. In the most basic case, this involves representing the empty weight W_e through an empty weight fraction, which is determined based on data for existing vehicles: $(W_e/W_o) = f(W_o)$. In a more detailed approach, the vehicle takeoff gross weight is expressed as the sum of the weights of major components, fuel, and payload: $W_o = \sum_i W_{comp,i} + W_{fuel} + W_{payload}$. The component weights themselves are expressed through relationships that typically take the form $W_{comp,i} = A(W_o)^a(P_1)^{x_1}\ldots(P_n)^{x_n}$, where $P_1, \ldots P_n$ are parameters on which the component's weight depends, and coefficients $A, a, x_1, \ldots, x_n$ are determined by fitting to existing data. Since the component weight equations typically contain the takeoff gross weight W_0 raised to some exponent, the implicit system of weight build-up equations is solved iteratively, starting with a guessed value of W_0, and iterating until the change in W_0 between iterations converges to below a suitable threshold.

The above iterative procedure to find W_0 is valid in general, however, the representation of the component weights in the form shown above requires that sufficient historical data be available to permit determination of the coefficients. This may not be the case for unconventional vehicle configurations, which do not conform to standard fixed-wing or rotary-wing vehicles configurations. In such cases, the direct applicability of standard/traditional weight estimation relationships may be questionable. To overcome this, a weight build-up approach that comprises a combination of physics-based weight assessments (through component sizing) as well as look-ups of component weights from available product data sheets may be attempted. This is especially relevant for the case of novel concepts such as roadable flight vehicles, whose configuration may be expected to contain some aircraft elements and some automobile elements. The weights of some other vehicle components are directly dependent on the assumed technological state-of-the-art. Examples include

weight estimation of electric motors and power electronics (based on gravimetric power densities, kW/kg), electric batteries (based on gravimetric energy density, Wh/kg), and so on. Thus, it is clear that to evaluate novel vehicle concepts, a highly flexible and parametric weight estimation approach is required.

To this end, a database of weight estimation relationships and techniques to cover major vehicle components, including structural elements, power-train elements, and energy storage system elements were created based on methods documented by Roskam [1] and NASA [33]. Table 1 summarizes the weight estimation method used in this work for each component. The first column lists the major components corresponding to Table A2.1a in Ref. [1]. The method used for each component is shown in the second column, where the Cessna method is given in Ref. [1], and the FLOPS method in Ref. [33]. Calibration factors associated with each major weight item were used to obtain reasonable agreement between the predicted weights and the aircraft's published weight breakdown (Table A2.1a of Ref. [1]).

Table 1. Methods used in estimating the aircraft empty weight breakdown

Component	Method	Primary Equations in Reference
Wing	Cessna	(5.2), (5.3)
Empennage	FLOPS	(48), (52)
Fuselage	Cessna	(5.23), (5.24)
Landing gears	Cessna	(5.38), (5.39)
Nacelle	N/A	N/A
Engine	FLOPS (modified)	(75)
Air induction system	N/A	N/A
Fuel system	FLOPS	(152)
Propeller	N/A	N/A
Engine installation	N/A	N/A
Flight control system	Cessna	(7.1)
Avionics and electrical systems	Cessna	(7.12)
Hydraulics	N/A	N/A
Furnishing	Cessna	(7.41)
Air conditioning	N/A	N/A
Anti-icing system	N/A	N/A

Among the components listed in Table 1, the engine weight was estimated by modifying a FLOPS equation [33] that originally scaled engine weight based on the thrust to use power instead. The baseline engine weight (W^*_{engine}) was scaled based on the ratio of desired power to baseline engine power ($P_{desired}/P_{baseline}$), as shown in Eq. 15:

$$\mathbf{W_{engine}} = W^*_{engine}\left(\frac{P_{desired}}{P_{baseline}}\right)^{1.15} \tag{15}$$

In Table 1, no appropriate weight estimation method is applicable to some components, such as the air induction system and the propeller. In these cases, the empty weight margin coefficient (K_{EW}) was used to group these component weights in a single term, as defined in Eqn. 16, where W_e is the empty weight of the baseline aircraft, and $W_{component\,i}$ is the sum of all computable component weights listed in Table 1, including the wing, empennage, fuselage, etc.

$$\mathbf{W_e} = (1 + K_{EW})\sum_i W_{component\,i} \tag{16}$$

Once K_{EW} was determined from the baseline aircraft, its value was held constant during the sizing process to account for the weight changes of the remaining components during vehicle sizing.

The baseline for the electric motor was selected to be the best in class Siemens 260 kW direct-drive electric motor (SP260D) which has a power-to-weight ratio of 5 kW/kg and scalable up to 1 MW [6, 34]. The

electric motor weight was calculated by dividing rated power by the power-to-weight ratio. The rechargeable battery was sized based on the total required energy for the design and reserve missions and a state-of-the-art gravimetric energy density of 250 Wh/kg. The interested reader is referred to Cinar et al. [35, 36] for more detailed description of the weight estimation and sizing of these electric propulsion system components. The electric motor and battery weights obtained in this manner were incorporated into the iterative weight convergence approach described above in order to estimate the vehicle empty and gross weights.

V. Vehicle Sizing and Synthesis

The sizing approach for vehicles with hybrid electric propulsion architectures is based on (i) matching the point performance (e.g. specified takeoff and landing field lengths, climb rate, and steady cruise speed, etc.) of the baseline aircraft, and (ii) an on-design mission analysis.

Point performance requirements are represented by sizing parameters such as power-to-weight ratio (P_{SL}/W_{TO}) and wing loading (W_{TO}/S). The lower limit of the former, for instance, may be driven by takeoff field length or climb gradient requirements. For GA vehicles, the upper limit of the latter may be driven by an upper bound on permissible approach speed or stall speed. In this work, the power-to-weight ratio and wing loading of sized vehicles were required to match those of the baseline vehicle. Thus,

1. Regardless of the propulsion system architecture, the overall power-to-weight ratio of the new design must be equal to or greater than that of the baseline aircraft, as shown in Eq. 17, where P_{SL} is the sea level maximum power of the aircraft at sea level, W_{TO} is the takeoff gross weight, and $P_{SL\,i}$ represents the sea level rated power of a power source i of the new aircraft.

$$\left(\frac{\mathbf{P_{SL}}}{\mathbf{W_{TO}}}\right)_{\mathbf{new}} = \left(\frac{\sum_i P_{SL\,i}}{W_{TO}}\right)_{new} \geqslant \left(\frac{P_{SL}}{W_{TO}}\right)_{baseline} \tag{17}$$

2. The candidate design must have the same design wing loading as the baseline, as shown in Eq. 18.

$$\left(\frac{\mathbf{W_{TO}}}{\mathbf{S}}\right)_{\mathbf{new}} = \left(\frac{W_{TO}}{S}\right)_{baseline} \tag{18}$$

The vehicle sizing is an iterative process, in which each iteration includes the recalculation of aircraft geometry, component weights, and the required energy of each energy source for the design and reserve missions. The following sections briefly describe the sizing of individual components, the overall iteration procedure, and convergence criteria.

A. Sizing of the Wing and Tail Geometry

In this work, the dimensions of the baseline vehicle's fuselage were maintained, but wings, horizontal tail, and vertical tails were resized. The wing is scaled through changing its planform area to match the baseline wing loading, as given by Eq. 18. The remaining geometric properties (such as taper ratio, aspect ratio, thickness-to-chord ratio, etc.) were held invariant. The empennage size is updated based on the tail volume coefficients using Eq. 19, where S_h and S_v are the areas of horizontal and vertical tails, c is the wing mean aerodynamic chord, S is the wing planform area, b is the wingspan, l_h and l_v are the lengths of the moment arms of the horizontal and vertical tails with respect to the aircraft center of gravity, and V_h and V_v are the horizontal and vertical tail volume coefficients.

$$S_h = \frac{Sc}{l_h}V_h, \qquad S_v = \frac{Sb}{l_b}V_b \tag{19}$$

B. Sizing of the Power Sources

According to the condition described in Eq. 17, the sum of sea level rated power of all the power sources on the new aircraft can be calculated for a given or previously computed takeoff gross weight. The distribution of this required rated power to all of the available power sources is then made by defining a *rated power split* (κ_i). This describes how much (percentage-wise) of the total sea level required power the power source i must deliver. For instance, for the parallel hybrid-electric propulsion architecture shown in Figure 1(b),

$\kappa_{EM} = 0.7$ means that the electric motor delivers 70% of the required sea level power of the aircraft. To match the total rated power to that of the baseline aircraft, the fuel-burning engine must then deliver the remaining 30%, i.e. $\kappa_{EM} = 0.3$.

Once the required sea level rated powers of the power sources are determined, each power source can be sized accordingly. In this work, the electric motor was sized based on a loss-based electric motor model, described by Lowry and Larminie [37]. The rubberized electric motor was sized such that while being able to deliver the required rated power, its maximum efficiency (which was taken to be 95%, similar to the SP260D [6]) occurred at the power required during cruise (the most dominant segment of the mission) in the on-design mission.

For the IC engine, data for existing IC engines was used. To avoid excessive scaling-up or scaling-down of a single engine's performance curves, a set of engine performance curves (fuel consumption versus output power and flight condition) was first obtained from different engine manuals (e.g., [38]). An algorithm was developed to first choose the performance curves of the reference engine with rated power closest to that of the current iteration, and then perform the limited scaling required to make said curves match the required power of the current iteration.

C. Sizing of the Propeller

An in-house propeller model based on the blade element momentum theory was used to estimate the performance of the propeller. The propeller of the baseline aircraft was modeled as a constant-speed, 76 inch, 2-bladed aluminum propeller, similar to that of Cessna 172 [26].

As the takeoff gross weight of the sized vehicle changes, the thrust required and hence the propeller size must change. Gudmundsson [39] gives a rapid estimation method to calculate the diameter (D) of metal propellers in inches based on the brake horse power (P_{BHP}), as given in Eq. 20.

$$\mathbf{D} = K_p \sqrt[4]{P_{BHP}} \tag{20}$$

In Eq. 20, the multiplier K_p was taken to be 22 for a two-bladed propeller, 18 for a three-bladed propeller and 16 for a four-bladed propeller.

The permissible propeller diameter is upper-bounded by ground clearance requirements and tip speed limitations. Starting with a 2-bladed propeller at first, if the required thrust cannot be met without encountering these two constraints, then the number of blades is increased (to 3-bladed and then 4-bladed) If the tip speed results in an unacceptably high tip Mach number, then the reference propeller RPM is reduced from that of the baseline.

D. Sizing of the Energy Sources

In this work, the energy sources are housed inside the wing. For a conventional airplane, the available volume inside the wing is used to house the fuel tanks. For the hybrid propulsion system architecture, part of this volume is allocated to the batteries. The internal available volume of the wing is computed using Eq. 21, based on [33], where K_{wv} is a dimensionless wing internal volume coefficient, (t/c) is the wing thickness-to-chord ratio, and λ is the wing taper ratio. The value of K_{wv} was first determined such that given the baseline aircraft wing geometry, Eq. 21 yields the fuel tank volume of the baseline aircraft. For a purely electric or a hybrid architecture, the volume taken up by the battery is determined by the required battery energy of the design and reserve missions and the volumetric energy density. For a hybrid architecture, the volume remaining after the placement of the battery is allocated to the fuel tanks.

$$\mathbf{V_W} = K_{wv} \frac{S^2}{b} \left(\frac{t}{c}\right) \left(1 - \frac{\lambda}{(1+\lambda)^2}\right) \tag{21}$$

In the case of insufficient volume left to hold the necessary fuel, the wing volume is increased by a small margin through an iteration process. This increase in the wing volume results in a heavier wing and hence the empty weight is updated.

E. The Iterative Sizing Process

The iteration steps, depicted through the process flowchart of Figure 2, can be summarized as follows:

1. Start with an initial guess for the takeoff gross weight and battery weight
2. Update the aircraft wing and empennage sizes (Section V .A)
3. Size the power sources (IC engine and electric motor) and the propeller (Section V .B
4. Calculate the empty weight at the first iteration, update at later iterations (Section V, Table 1)
5. Recalculate the aircraft gross weight based on the empty weight obtained at the previous step
6. Check whether the newly calculated gross weight and the initially estimated gross weight converge to each other within a reasonable margin of error
   (a) If not converged, start the inner iteration process (iteration *i*, framed by the blue dashed line) by returning to step (2)
   (b) If converged, move on to step (7)
7. Fly the design mission to evaluate the total energy required to fly the given mission profile (Section III)
8. Update the fuel and battery weights based on the individual energy requirements from each energy source
9. Recalculate the aircraft gross weight
10. Check whether the newly calculated gross weight and the gross weight obtained at the end of iteration (i) converge to each other within a reasonable margin of error
    (a) If not converged, move on to the next iteration beginning from step (2)
    (b) If converged, freeze the final vehicle design and end the iteration process

Once the outer iteration loop (iteration *ii*, framed by the red dashed line) converges, the resulting vehicle design is frozen. The performance of the sized vehicle can then be evaluated over off-design missions, where gross weight and empty weight are kept constant but tradeoffs can be made between fuel and payload weights.

VI. Optimization

Comparisons among different hybrid electric architectures are meaningful only if they are operated under their optimum performance [40]. The following sections describe the approach to computing the optimal power management strategy.

A. Objective Function Selection

Minimum fuel burn, maximum range, minimum emissions, and so on are all valid objective functions. The most common objective in hybrid electric automobile applications is to optimize for minimum fuel consumption [40–43]. However, automobiles have different characteristics than aircraft, which leads to different priorities for the optimization problem. Hence, similar work in this field can be leveraged, but it cannot be directly applied to the problem at hand.

Minimizing fuel consumption is a major concern in aerospace community, and is the major motivation of EA/HEA efforts. Interesting trade-offs are expected to come out of such a study, especially when an aircraft is to be flown different ranges than its design range. Minimization of fuel burn leads to an increase in required electrical energy. For long ranges, the required energy might be so high that an extremely heavy battery with large capacity is required. However, a heavy battery can significantly increase the power requirement, as the specific energy of batteries are significantly lower than conventional fuel. After some point, this might lead to even more fuel consumption compared to a lower level of hybridization, and hence the optimizer might decide in favor of a conventional-like propulsion with low level of hybridization, if at all. On the other hand, optimizing for minimum fuel consumption for short range missions might result in high levels of hybridization or a fully electric aircraft.

Most system level requirements are tied to energy consumption. However, if the objective of the optimization problem is chosen to be minimum energy required, then the optimizer would most probably decide

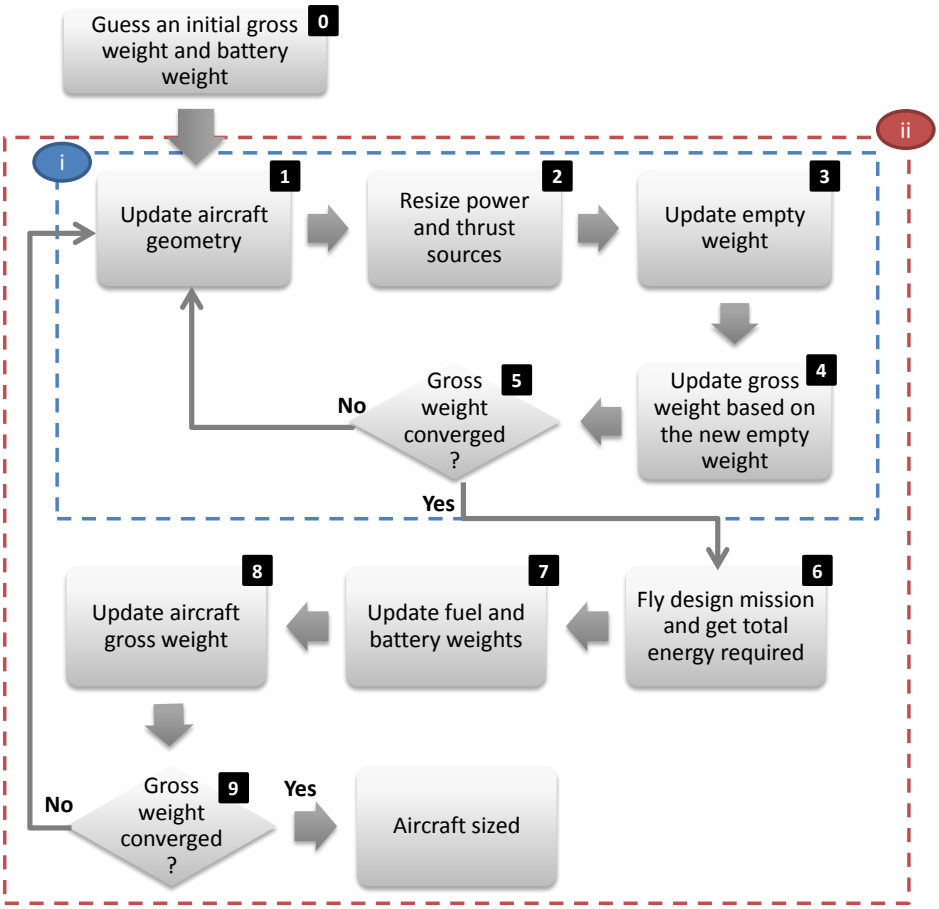

Figure 2. Vehicle sizing flowchart with an inner and an outer iteration process on takeoff gross weight convergence.

on a conventional architecture with no electrification because of the significantly lower specific energy of current batteries compared to conventional fossil fuels.

For similar reasons, another interesting objective could be to minimize energy expenditure per distance. A long range mission automatically requires more energy than a short range mission, and therefore it would not make sense to compare the two. However, if energy consumption is normalized by distance, then a comparison is made possible. This approach is similar to that of automobiles, where "miles per gallon" is a significant factor for efficiency.

Since weight is a major concern for aircraft, it would also be interesting to solve an optimization problem for minimizing the takeoff gross weight (TOGW or W_{TO}). Optimizing for TOGW inherently deals with fuel weight, battery weight, engine weight, EPGDS weight, and weight of other structural components. Moreover, it is also a function of how the aircraft is operated. The results can be compared with fuel optimized designs. Instead of formulating a single-objective optimization using an Overall Evaluation Criterion through the weighted summation of multiple objectives, a multi-objective optimization approach can be used to reveal non-dominated Pareto-optimal designs.

B. Design and Control Variables

In an optimal power management solution, while the power contribution of the different sources can vary over time and over different mission segments, the variation is likely to be smooth and there is no physical reason to expect rapid and abrupt variations over short intervals of time. Therefore, the optimization problem does not have to be explicitly solved for each and every instant of time over the mission. Rather, a few strategically-chosen control points may be used to represent the overall variation of the power contributions

over the course of the mission. With this in mind, two types of optimization scenarios can be addressed:

1. Optimal sizing and operation of the aircraft over a design mission
2. Optimal operation of the sized aircraft over off-design mission(s)

Table 2 shows the design/control variables pertinent to these two scenarios.

Table 2. List of design and control variables for design and off-design missions

Design/Control Variables		Design Mission Optimization	Off-design Mission Optimization
Wing planform design variables	Wing area, wing span, taper ratio, sweep	✓	✗
Propulsion system design sizing variables	Total sea level rated power; Sea level rated power split	✓	✗
Power management control variables	$u_1, u_2, \ldots, u_n$	✓	✓

While the goal is to find the optimum hybridization schedule, the hybridization factor may not directly be a suitable control variable, since (i) not all hybridization factors may be realizable at all flight conditions given engine power lapses and (ii) the hybridization factors for climb and cruise segments were defined differently (Eq. 8 and Eq. 11).

Instead, the two alternative control variables that are employed are electric motor normalized power, $u_{EM}(t)$, and fuel burning engine normalized power, $u_{FB}(t)$, as defined in Eq. 22 and Eq. 23, respectively. These variables are set for each power source at each control point, yielding a total of n control variables.

$$\mathbf{u_{EM}}(\mathbf{t}) = \frac{P_{EM,req}(t)}{P_{EM,max\,av}} \tag{22}$$

$$\mathbf{u_{FB}}(\mathbf{t}) = \frac{P_{FB,req}(t)}{P_{FB,max\,av}} \tag{23}$$

In Eq. 22 and Eq. 23, $P_{EM,req}(t)$ and $P_{FB,req}(t)$ are instantaneous required power from the electric motor and IC engine, and $P_{EM,max\,av}$ and $P_{FB,max\,av}$ are the maximum available power of the electric motor and the IC engine at a given flight condition, respectively. Note that the value of $P_{FB,max\,av}$ varies with altitude. Then, the following invariant bounds apply to the control variables:

$$0 \leq u_{EM}(t) \leq 1$$

$$0 \leq u_{FB}(t) \leq 1$$

Once $u_{EM}(t)$ and $u_{FB}(t)$ are found for an optimal design, required electric motor and fuel-burning engine power can be calculated directly from Eq. 22 and Eq. 23. Thereafter, hybridization factor for each power source at each control point can be computed from Eq. 8 and Eq. 11.

Once the optimal values of the control and design variables are found for the design mission, the wing planform variables, engine power rating (and hence the engine weight), and electric motor power rating (and hence the electric motor weight) can be determined and fixed. Optimization of off-design mission performance is performed using only the control variables that determine the power split between fuel-burning and electric power paths.

C. Optimization Constraints

As mentioned previously, point performance constraints were implicitly accounted for by requiring the wing loading and power-to-weight ratio of the hybrid electric aircraft to match those of the baseline. Basic mission segment constraints such as minimum rate of climb, minimum time to climb, minimum permissible block speed during cruise, and reserve energy requirements were also imposed. Additionally, the following constraints were applied for the hybridization factor of each power source:

$$0 \leq \lambda_i \leq 1, \qquad \forall \lambda_{climb} \;\&\; \forall \lambda_{cruise}$$
$$\sum_i \lambda_{cruise,\,i} = 1$$

where, similar to $u_{EM}(t)$ and $u_{FB}(t)$, the minimum limit (0) indicates zero power, and the maximum limit (1) indicates maximum available power for the associated power source at the relevant flight condition.

VII. Demonstration of an Example Application of the Developed Framework

The sizing and optimization approach described in this work is demonstrated for the case of a parallel hybrid electric architecture and over a mission profile consisting of simple takeoff-climb-cruise-descent-land schedule, accompanied by a 30-minutes reserve mission. Both main and reserve missions were flown with the following objectives: (i) minimum time to climb to the best SAR altitude, (ii) best specific air range cruise, and (iii) descent with minimum equilibrium glide angle. The useful payload for the design mission was set to a fixed weight of 160 kg.

A. Sensitivity of Mission Performance to Uncertainties

Prior to optimization, the sensitivity of vehicle sizing to the following parameters was established:

- Power management schedule during the mission through hybridization factors
- Rated power split of the power sources
- Technological state-of-the-art for the gravimetric energy density of the battery
- Design mission range

The bounds over which these parameters or K-factors were varied are given in Table 3.

Table 3. Upper and lower boundaries of the design variable space of K-factors used in the sensitivity analysis

Design Variables	Minimum Limit	Maximum Limit	Units
Hybridization factor for electric motor at climb	0	1	-
Hybridization factor for IC engine at climb	0	1	-
Hybridization factor for IC engine at cruise	0	1	-
Rated power split	0	100	%
Battery gravimetric energy density	0.2	0.5	kWh/kg
Design mission range	50	500	nmi

The rated power split was defined to be the percentage rated power of the electric motor compared to the rated power of the baseline aircraft's engine. The hybridization factor at cruise $\lambda_{cruise,EM}$ for the electric motor was not included in the design variable space as it can easily be computed using Eq. 24.

$$\lambda_{\mathbf{cruise,EM}} = 1 - \lambda_{cruise,ICE} \tag{24}$$

The sensitivity studies were performed with hybridization factors kept constant within the climb and cruise segments, regardless of a power lapse in the IC engine. When the hybridization factor of the electric

motor for both the climb and cruise segments take the value of zero (0), then this case represents the conventional propulsion where the only power and energy sources are the IC engine and fossil fuel. In this case, the only allowed value that the rated power split can take is 0%. Similarly, when the electric motor hybridization factor is 100% for both of the mission segments, then this case represents a fully electric flight driven by the electric motor (where the rated power split can only be 100%) and the rechargeable battery.

The battery gravimetric energy density was extrapolated from today's available density figures for the rechargeable Lithium-Ion batteries. It must be emphasized that the maximum limit of 1 kWh/kg for the energy density is not realistic neither with today's technology nor for near future, but was included to understand where battery technology would need to be for EA/HEA to have similar performance to the conventional GA vehicles, especially in terms of trip distance and flight endurance characteristics.

Finally, the design range for the on-design mission was varied from 50 nmi to 500 nmi. The upper limit on the range is similar to that of Cessna 172 with the same payload weight. However, the current battery technology would not allow for fully or mostly electric flights for the same design range of conventional GA-type aircraft. To find out a more appropriate design range for such vehicles, a literature study on on-demand electric aviation was made and it was revealed that there is a potential for such vehicles to disrupt short-range trips in the future, as around 30% of all U.S. travel is made between 100 to 300 nautical miles, where by ground transportation (automobiles) currently dominates [44, 45]. Moreover, urban air mobility concepts are envisioned to fly a typical trip distance of around 25 nautical miles, and sized to a maximum range of 50 nautical miles [14].

A custom-made design of experiments (with a total of over 3500 samples including all of the corner points and some of the interior points in the design space) was conducted to sample data within the ranges of all K-factors. A Neural Network model was constructed for each of the key performance metrics: the takeoff gross weight, total energy required, specific air range (SAR), total fuel weight, and battery weight. These models were tested for goodness of the fit and validated against data which were not used to create the surrogate models. Finally, a sensitivity study was performed to analyze the impact of these K-factors on the metrics of interest. The results of this sensitivity study are given in Figure 3.

In Figure 3, the x-axes correspond to the varied K-factors, while the y-axes correspond to the vehicle sizing responses of interest. The values shown in red on the horizontal axis are the median values within the ranges of each K-factor. The values shown in red on the vertical axis are corresponding predicted responses at those K-factor settings. The slopes of the lines indicate the relative sensitivity of a y-axis response to variation of an x-axis K-factor, with other K-factors held fixed (essentially equivalent to partial derivatives of the responses with respect to the K-factors).

It can be easily seen from Figure 3 that for the selected K-factor and hybridization factor settings in (shown in red on the vertical axes), higher range values are mostly impractical due to the extremely high values of gross weight.In fact, when sized to the same payload capability and maximum takeoff weight as the conventional baseline, the range capability of the hybrid design is reduced significantly to 60 nautical miles with the given settings.

Figure 3 also reveals that the power management strategy plays a significant role especially in terms of specific air range (SAR). Greater use of the electric propulsion system during cruise (i.e. decreasing $\lambda_{ICE,\,cruise}$ results in a heavier aircraft which is significantly less efficient in terms of energy expenditure per unit of distance flown (i.e. lower SAR).

The up-and-down trend seen in fuel weight with respect to electric motor rated power split is due to changing IC engine decks based on the required power rating from the IC engine, as explained in Section V. B. Gross weight also drops with increasing electric motor rated power split as the electric motor power-to-weight-ratio as well as the efficiency are much larger than that of the IC engine.

B. Design Mission Optimization

An example design mission optimization was solved based on the optimization problem defined in Section VI to minimize the following objectives:

- Design 1: Fuel required
- Design 2: Energy required
- Design 3: Takeoff gross weight

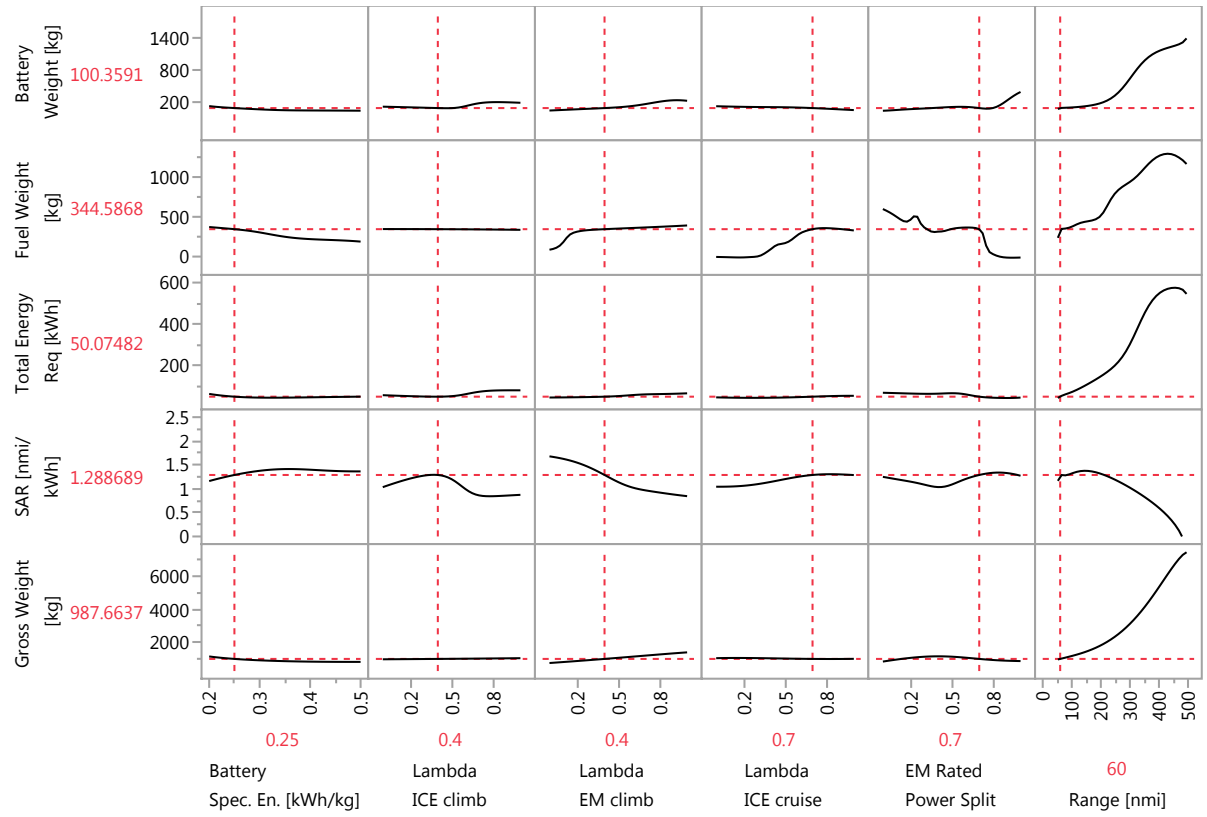

Figure 3. Prediction profiler showing sensitivity of vehicle sizing to variation of K-factors (Total energy includes energy required for both main and reserve missions)

For this analysis, four control points were selected: at the beginning and end of the climb, and at the beginning and end of the cruise segments. Then, a pattern search based optimizer was provided an initial design with guessed values for the control variables. This optimizer calls the mission analysis which evaluates the value of the objective function at the given control points. The optimizer perturbs the control variables at the control points until the objective function is minimized. The control variable values in between the control points are obtained by linear interpolation. The remaining K-factors and mission profile parameters were selected as follows:

- The rechargeable battery has a specific energy of 0.25 kWh/kg
- The electric motor rated power split is set to different values for different architectures as: 60% for hybrid-electric, 0% for fully conventional, and 100% for fully electric designs
- Payload weight, wing loading, and power loading values match those of the baseline aircraft
- Design mission range is 100 nautical miles (in addition to a 15 minutes long reserve mission)
  - Climb segment objective is minimum time to climb for the main mission; minimum energy to climb for the reserve mission
  - Cruise segment objective is best specific air range
  - Descent segment objective is minimum equilibrium glide angle

An IC engine powered aircraft was sized based on the same baseline aircraft properties for a 100 nautical miles of design range to compare the resulting optimized vehicles for each objective function in terms of a list of design properties shown in Table 4. The accompanying optimized control variables are presented in Figure 4 throughout the mission profile. Each mission profile is different as each design was optimized to fly based on the aforementioned mission segment objectives.

Table 4. Comparison of the baseline aircraft to the new HEA design optimized for minimum fuel consumption and minimum energy required to fly the 100 nautical miles design mission and 15 minutes long reserve mission. Design 3 is not shown in this table due to insignificant variation from the baseline aircraft.

Design Variable	Baseline	Design 1 (min fuel)	Design 2 (min energy)
TOGW [kg]	693.7	991.8	1401.2
Change over baseline	-	*+43.0%*	*+102.0%*
Fuel Weight [kg]	11.8	10.1	271.1
Change over baseline	-	*-14.4%*	*+2197.5%*
Battery Weight [kg]	N/A	226.3	225.9
Energy Required [kWh]	56.6	56.0	53.8
Change over baseline	-	*-1.1%*	*-4.9%*
IC Engine Rated Power [kW]	84.0	72.0	55.5
Change over baseline	-	*-14.3%*	*-33.9%*
Electric Motor Rated Power [kW]	N/A	61	70.5
Propeller diameter [m]	1.3 (2-bladed)	1.5 (2-bladed)	1.6 (4-bladed)
Change over baseline	-	*+15.4%*	*+23.1%*
Wing Area [m^2]	11.3	16.1	22.7
Change over baseline	-	*+42.5%*	*+100.9%*
Wing loading [N/m^2]	605.6	605.6	605.6
Power loading [kW/kg]	0.12	0.12	0.12

Design 3 is not explicitly shown in Table 4 because of the fact that the resulting optimized vehicle ended up almost identical with the baseline aircraft, implying that the minimum takeoff gross weight is obtained when the aircraft does not run on electric energy. In fact, none of the optimized designs obtained significant advantage over the baseline aircraft in terms of the listed design variables. On the contrary, the baseline aircraft with conventional propulsion is the lightest, smallest design that requires only slightly more fuel than the hybrid electric Design 1 which was optimized for minimum fuel consumption.

Although a hybrid electric propulsion system turned out to be disadvantageous for a range of 100 nautical miles with current battery technology, it's advantages can be seen when the same optimization objectives are solved for an otherwise identical mission with of a design range of 50 nautical miles, similar to the aforementioned urban air mobility type concepts [14]. The results are given in Table 5. The accompanying optimized control variables are presented in Figure 5 throughout the mission profile. Again, each mission profile is different as each design was optimized to fly based on the aforementioned mission segment objectives.

For the optimization for a range of 50 nautical miles, Design 3 (optimized for minimum TOGW) yielded almost identical results to that of baseline, similar to the previous case. However, a very interesting result was obtained by solving the optimization problem for minimum fuel required. Design 2 turned out to be a completely electric aircraft, without any fuel or internal combustion engine. This design yields fuel savings for a reasonable vehicle size and gross weight. Design 2, which is the optimized design for minimum energy required to fly the given mission, turned out to be in the middle of the baseline and Design 1 in terms of gross weight, but at a very high fuel weight expense.

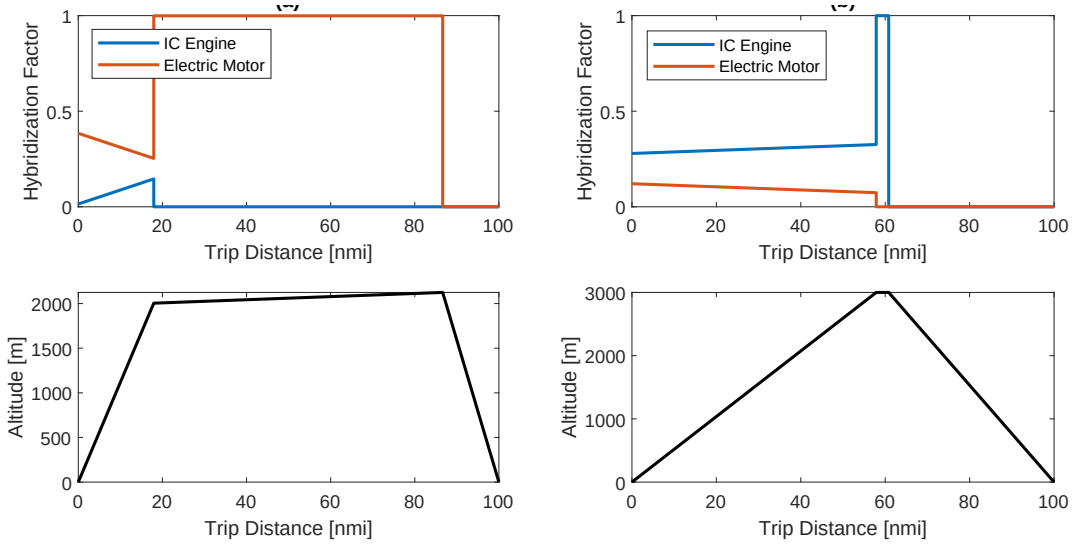

Figure 4. Variation of the optimized power management schedules for (a) Design 1, and (b) Design 2 with altitude and trip distance for the 100 nautical miles design mission. Refer to Eq. 8 and Eq. 11 for the hybridization factor definitions, as the definitions are different for climb and cruise segments.

VIII. Conclusion

This paper demonstrated the initial implementation of an approach that will ultimately allow the rapid sizing and analysis of novel aircraft concepts and propulsion system architectures. A salient feature of the demonstrated approach is that the mission performance analysis is geared towards propulsion systems with more than one power/energy source, and as such, no cumbersome workarounds are required. The approach is demonstrated by sizing a General Aviation aircraft with a parallel hybrid electric propulsion system architecture over multiple design ranges where, in addition to the usual aircraft-level design parameters, control variables representing the relative power contributions of electric and conventional engines are also optimized with respect to two objective functions. Future extensions to this work will account for additional sizing constraints, a more detailed mission definition, an improved weight buildup capability, and additional optimizations and technology trade studies.

IX. Acknowledgments

The authors would like to thank Mr. Syed H. W. Gilani for supporting this work through his research on general aviation weight estimation methods, and Mr. Evan D. Harrison for providing the aforementioned propeller models.

Table 5. Comparison of the baseline aircraft to the new HEA design optimized for minimum fuel consumption and minimum energy required to fly the 50 nautical miles design mission and 15 minutes long reserve mission. Design 3 is not shown in this table due to insignificant variation from the baseline aircraft.

Design Variable	Baseline	Design 1 (min fuel)	Design 2 (min energy)
TOGW [kg]	684.8	866.2	779.4
Change over baseline	-	*+26.5%*	*+13.8%*
Fuel Weight [kg]	7.1	0	56.1
Change over baseline	-	*-100.0%*	*+690.1%*
Battery Weight [kg]	N/A	161.5	56.6
Energy Required [kWh]	35.7	33.2	26.4
Change over baseline	-	*-7.0%*	*-26.1%*
IC Engine Rated Power [kW]	82.6	0	44.0
Change over baseline	-	*-100.0%*	*-46.7%*
Electric Motor Rated Power [kW]	N/A	103.9	55.9
Propeller diameter [m]	1.3 (2-bladed)	1.4 (4-bladed)	1.4 (2-bladed)
Change over baseline	-	*+7.7%*	*+7.7%*
Wing Area [m^2]	11.1	14.0	12.6
Change over baseline	-	*+26.1%*	*+13.5%*
Wing loading [N/m^2]	605.6	605.6	605.6
Power loading [kW/kg]	0.12	0.12	0.12

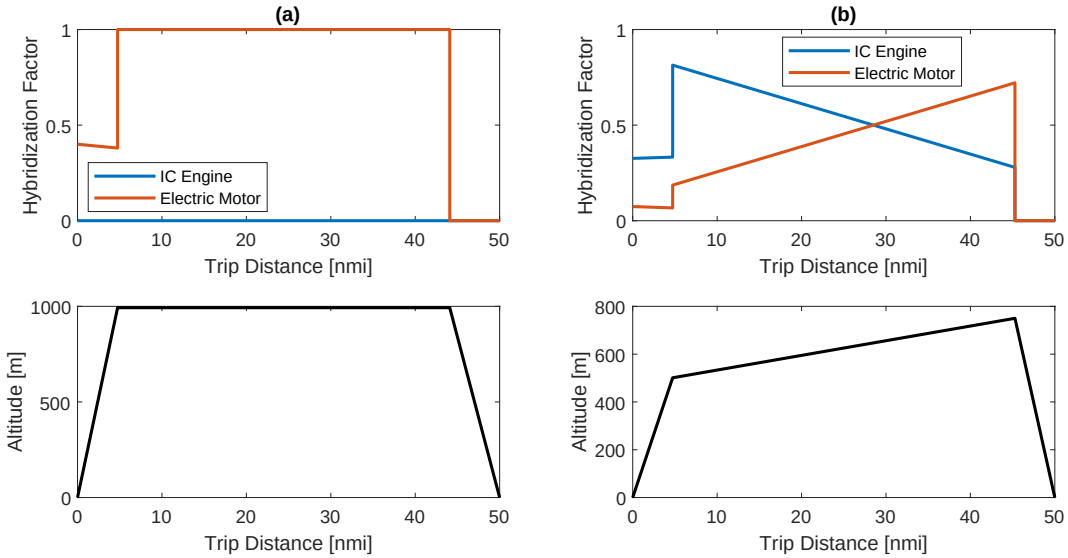

Figure 5. Variation of the optimized power management schedules for (a) Design 1, and (b) Design 2 with altitude and trip distance for the 50 nautical miles design mission. Refer to Eq. 8 and Eq. 11 for the hybridization factor definitions, as the definitions are different for climb and cruise segments.

References

[1] Roskam, J., *Airplane Design Part V - Component Weight Estimation*, Design Analysis and Research Corporation, Kansas, 1999.

[2] Torenbeek, E., *Synthesis of Subsonic Airplane Design: An Introduction to the Preliminary Design of Subsonic General Aviation and Transport Aircraft, with Emphasis on Layout, Aerodynamic Design, Propulsion and Performance*, Delft University Press, 1976.

[3] Hileman, J. I., Donohoo, P. E., and Stratton, R. W., "Energy content and alternative jet fuel viability," *Journal of propulsion and Power*, Vol. 26, No. 6, 2010, pp. 1184–1196.

[4] Tarascon, J.-M. and Simon, P., *Electrochemical Energy Storage*, Vol. 1, Wiley-ISTE, Somerset, US, Feb. 2015.

[5] Pipistrel, "Alpha Electro Overview," [company website], URL: `http://www.pipistrel.si/plane/alpha-electro/overview` [cited on 13 Sep 2015].

[6] Petermaier, K., "Electric propulsion components with high power densities for aviation," Transformative Vertical Flight Workshop, Siemens AG, 2015.

[7] Borer, N. K., Nickol, C. L., Jones, F., Yasky, R., Woodham, K., Fell, J., Litherland, B., Loyselle, P., Provenza, A., Kohlman, L., et al., "Overcoming the Adoption Barrier to Electric Flight," 54th AIAA Aerospace Sciences Meeting, AIAA, 2016.

[8] Airbus Group, "E-Fan Electric Aircraft," [company website], URL: `http://www.airbusgroup.com/int/en/corporate-social-responsibility/airbus-e-fan-the-future-of-electric-aircraft.html` [cited on 1 Mar 2017].

[9] Extra Aircraft, "The -Extra330 LE- Test Aircraft - Powered By Siemens 260kW Electric Engine - Made It's First Flight," [company website], July 2016, URL: `https://www.extraaircraft.com/news.php?quale_news=39&lang=4&tipo=&tutte=` [cited on 27 October 2017].

[10] Extra Aircraft, "Electric-flight record heralds new era of aviation," [press release], December 2016, URL: `https://www.extraaircraft.com/allegati/Press_Release_Extra-Electric-Aircraft_7Dec2016.pdf` [cited on 27 October 2017].

[11] Aurora Flight Sciences, "eVTOL," [company website], URL: `http://www.aurora.aero/evtol/` [cited on 27 October 2017].

[12] Aurora Flight Sciences, "LightningStrike XV-24A Demonstrator Successfully Completes Subscale Flight Test Program," [company website], URL: `http://www.aurora.aero/wp-content/uploads/2017/04/APR-340_LightningStrike-XV-24A.pdf` [cited on 27 October 2017].

[13] Aurora Flight Sciences, "XV-24A LightningStrike," [company website], URL: `http://www.aurora.aero/lightningstrike/` [cited on 27 October 2017].

[14] Airbus Group, "Uber Elevate Mission and Vehicle Requirements," [company website], URL: `https://www.uber.com/info/elevate/` [cited on 17 May 2018].

[15] Volocopter, "Design specifications Volocopter 2X," [company website], April 2017, URL: `https://www.volocopter.com/assets/pdf/2017_04_Design_specifications_2X.pdf` [cited on 27 October 2017].

[16] Lilium, "Lilium Jet," [company website], URL: `https://lilium.com` [cited on 27 October 2017].

[17] Nam, T., Soban, D., and Mavris, D., "Power based sizing method for aircraft consuming unconventional energy," 43rd AIAA Aerospace Sciences Meeting and Exhibit, AIAA, Reno, NA, Jan. 2005.

[18] Nam, T., Soban, D., and Mavris, D., "A generalized aircraft sizing method and application to electric aircraft," 3rd International Energy Conversion Engineering Conference, AIAA, San Francisco, CA, Aug 2005.

[19] Pornet, C., Gologan, C., Vratny, P. C., Seitz, A., Schmitz, O., Isikveren, A. T., and Hornung, M., "Methodology for sizing and performance assessment of hybrid energy aircraft," *Journal of Aircraft*, Vol. 52, No. 1, 2014, pp. 341–352.

[20] Isikveren, A. T., Seitz, A., Vratny, P. C., Pornet, C., Plötner, K. O., and Hornung, M., "Conceptual studies of universally-electric systems architectures suitable for transport aircraft," Deutscher Luft-und Raumfahrt Kongress, DLRK Berlin, Germany, Sep. 2012.

[21] Perullo, C. and Mavris, D., "A review of hybrid-electric energy management and its inclusion in vehicle sizing," *Aircraft Engineering and Aerospace Technology: An International Journal*, Vol. 86, No. 6, 2014, pp. 550–557.

[22] Moore, M. D., "Misconceptions of Electric Aircraft and their Emerging Aviation Markets," 52nd Aerospace Sciences Meeting, AIAA, National Harbor, Maryland, 13-17 Jan. 2014.

[23] Borer, N. K., Patterson, M. D., Viken, J. K., Moore, M. D., Bevirt, J., Stoll, A. M., and Gibson, A. R., "Design and Performance of the NASA SCEPTOR Distributed Electric Propulsion Flight Demonstrator," 16th AIAA Aviation Technology, Integration, and Operations Conference, AIAA, Washington, D.C., June 2016.

[24] McCullers, L. A., *FLOPS User's Guide*, NASA Langley Research Center, Hampton, VA, 8th ed., October 2009.

[25] Antcliff, K. R., Guynn, M. D., Marien, T., Wells, D. P., Schneider, S. J., and Tong, M. J., "Mission Analysis and Aircraft Sizing of a Hybrid-Electric Regional Aircraft," *54th AIAA Aerospace Sciences Meeting*, 2016, p. 1028.

[26] Cessna Aircraft Company, "Pilot's Operating Handbook: Skyhawk Cessna Model 172N," 1978.

[27] Chau, K. and Wong, Y., "Overview of Power Management in Hybrid Electric Vehicles," *Energy Conversion and Management*, Vol. 43, No. 15, 2002, pp. 1953–1968.

[28] Khajepour, A., Fallah, M. S., and Goodarzi, A., *Wiley Desktop Editions : Electric and Hybrid Vehicles : Technologies, Modeling and Control - A Mechatronic Approach*, Wiley, Feb. 2014.

[29] Amelink, M. H., Mulder, M., Van Paassen, M., and Flach, J., "Theoretical Foundations for a Total Energy-Based Perspective FlightPath Display," *International Journal of Aviation Psychology*, Vol. 15, No. 3, 2005, pp. 205–231.

[30] Puranik, T., Jimenez, J., and Mavris, D., "Energy-Based Metrics for Safety Analysis of General Aviation Operations," *Journal of Aircraft*, 2017.

[31] Kumar, B., DeRemer, D., and Marshall, D., editors, *An Illustrated Dictionary of Aviation*, The McGraw-Hill Companies, Inc., 2005.

[32] Anderson, J. D., *Aircraft Performance and Design*, The McGraw-Hill Companies, Inc., 1999.

[33] Wells, D. P., Horvath, B. L., and McCullers, L. A., *The Flight Optimization System Weights Estimation Method*, Vol. 1, NASA, June, NASA/TM?2017?219627.

[34] Siemens AG, "World-record Electric Motor For Aircraft," [company website], Mar. 2015, URL: `http://www.siemens.com/press/en/feature/2015/corporate/2015-03-electromotor.php?content[]=Corp` [cited on 13 Sep. 2015].

[35] Cinar, G., Mavris, D. N., Emeneth, M., Schneegans, A., and Fefermann, Y., "Development of Parametric Power Generation and Distribution Subsystem Models at the Conceptual Aircraft Design Stage," 55th AIAA Aerospace Sciences Meeting, AIAA SciTech Forum, AIAA, Grapevine, TX, Jan. 2017.

[36] Cinar, G., Mavris, D. N., Emeneth, M., Schneegans, A., Riediger, C., Fefermann, Y., and Isikveren, A., "Sizing, Integration and Performance Evaluation of Hybrid Electric Propulsion Subsystem Architectures," 55th AIAA Aerospace Sciences Meeting, AIAA SciTech Forum, AIAA, Jan. 2017.

[37] Lowry, J. and Larminie, J., *Electric Vehicle Technology Explained*, John Wiley & Sons, 2nd ed., June 2012.

[38] Lycoming, *Operator's Manual: O-360, HO-360, IO-360, AIO-360, HIO-360 and TIO-360 Series*, Williamsport, PA, 8th ed., Oct 2005.

[39] Gudmundsson, S., *General Aviation Aircraft Design: Applied Methods and Procedures*, Elsevier Inc., Waltham, MA, 1st ed., 2014, ISBN: 978-0-12-397308-5.

[40] Kim, N., Cha, S., and Peng, H., "Optimal control of hybrid electric vehicles based on Pontryagin's minimum principle," *IEEE Transactions on Control Systems Technology*, Vol. 19, No. 5, 2011, pp. 1279–1287.

[41] Pisu, P. and Rizzoni, G., "A comparative study of supervisory control strategies for hybrid electric vehicles," *IEEE Transactions on Control Systems Technology*, Vol. 15, No. 3, 2007, pp. 506–518.

[42] Musardo, C., Rizzoni, G., Guezennec, Y., and Staccia, B., "A-ECMS: An adaptive algorithm for hybrid electric vehicle energy management," *European Journal of Control*, Vol. 11, No. 4-5, 2005, pp. 509–524.

[43] Sciarretta, A., Back, M., and Guzzella, L., "Optimal control of parallel hybrid electric vehicles," *IEEE Transactions on control systems technology*, Vol. 12, No. 3, 2004, pp. 352–363.

[44] Moore, M. D., "The Third Wave of Aeronautics: On-Demand Mobility," *SAE Technical Paper*, 2006, https://doi.org/10.4271/2006-01-2429.

[45] Moore, M. D., "Aviation Frontiers: On-Demand Aircraft," 10th AIAA Aviation Technology, Integration, and Operations (ATIO) Conference, AIAA, Fort Worth, TX, Sep. 2010.